ACCOUNTS of chemical research

pubs.acs.org/accounts Article

# Electrochemistry of Multilayer Electrodes: From the Basics to Energy Applications

Minsu Gu and Byeong-Su Kim*

Cite This: https://dx.doi.org/10.1021/acs.accounts.0c00524 Read Online



**CONSPECTUS:** Growing environmental concern has increased the demand for clean energy, and various technologies have been developed to utilize renewable energy sources. With the development of highly efficient energy conversion and storage systems, fundamental studies on the electrochemistry of electrodes are critical because the functionality of most of these systems relies on interfacial electrochemical reactions that occur on the surfaces of the electrodes. In this context, efficient electrode design methods are required to study specific electrochemical principles and the mechanisms of interfacial reactions on the surface of electrodes.

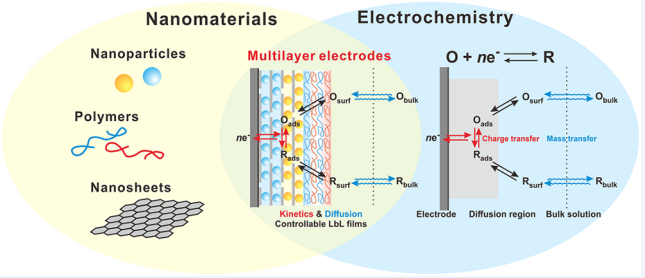


Compared with other electrode fabrication methods, layer-by-layer (LbL) assembly is a simple, inexpensive, and versatile process for producing highly ordered multilayer thin-film electrodes from a diverse array of materials. LbL-assembled multilayer electrodes exhibit distinct electrochemical properties compared with electrodes created via other fabrication methods because of the nanoscale control of the composition and structures of electrodes afforded by LbL assembly. LbL assembly can generate unique nanoarchitectures from a multiplicity of electroactive components to investigate the detailed electrochemical mechanisms within the electrode, allowing for investigations of the internal-architecture-dependent electrochemical properties within the electrodes. As electrochemical LbL research has progressed over the last 10 years, our group has performed pioneering studies on the fundamental electrochemical properties of multilayer electrodes fabricated via LbL assembly for diverse energy applications. In this Account, we aim to outline the fundamental electrochemistry occurring at the nanoscale level on multilayer thin-film LbL electrodes using our work to illustrate these concepts, including the dependence of the electrochemistry on the thickness and architecture of multilayer electrodes, competition between mass and charge transfer, and control over the ion-permeation selectivity and interfacial dipole moments in multilayer electrodes. We anticipate that our approach to LbL-assembled electrodes will be of great interest and provide an attractive platform for the investigation of fundamental multilayer thin-film electrochemistry. We also believe that it will provide guidelines for research efforts toward future electrode engineering.



## KEY REFERENCES


- Jo, K.; Gu, M.; Kim, B.-S. Ultrathin Supercapacitor Electrode Based on Reduced Graphene Oxide Nanosheets Assembled with Photo-Cross-Linkable Polymer: Conversion of Electrochemical Kinetics in Ultrathin Films. *Chem. Mater.* **2015**, *27*, 7982−7989.[1] *Charge transfer was facilitated after cross-linking within multilayer electrodes along with conversion of the electrochemical kinetics from charge transfer to mass transfer as the thickness of the multilayer electrode increased.*
- Gu, M.; Kim, B.-S. Unraveling the Importance of Controlled Architecture in Bimetallic Multilayer Electrode toward Efficient Electrocatalyst. *Nano Energy* **2016**, *30*, 658−666.[2] *The architecture dependence between charge transfer and mass transfer of Au- and Pd-based multilayer electrodes was demonstrated in the two-step methanol oxidation reaction.*
- Park, M.; Gu, M.; Kim, B.-S. Tailorable Electrocatalytic 5-Hydroxymethylfurfural Oxidation and $H_2$ Production: Architecture−Performance Relationship in Bifunctional Multilayer Electrodes. *ACS Nano* **2020**, *14*, 6812−6822.[3] *The sequential multistep oxidation of 5-hydroxymethylfurfural can be highly affected by changing the thickness and relative position of the metal nanoparticle catalysts within multilayer electrodes for each type of reaction kinetics.*


Received: August 14, 2020




https://dx.doi.org/10.1021/acs.accounts.0c00524
Acc. Chem. Res. XXXX, XXX, XXX−XXX

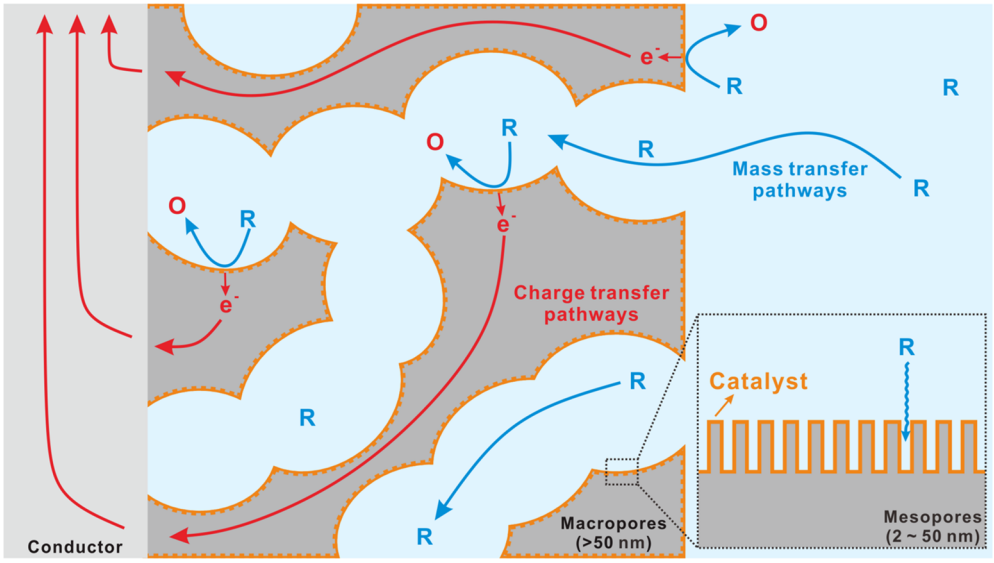


**Figure 1.** Various electrochemical reactions in macro- and mesoporous electrodes.

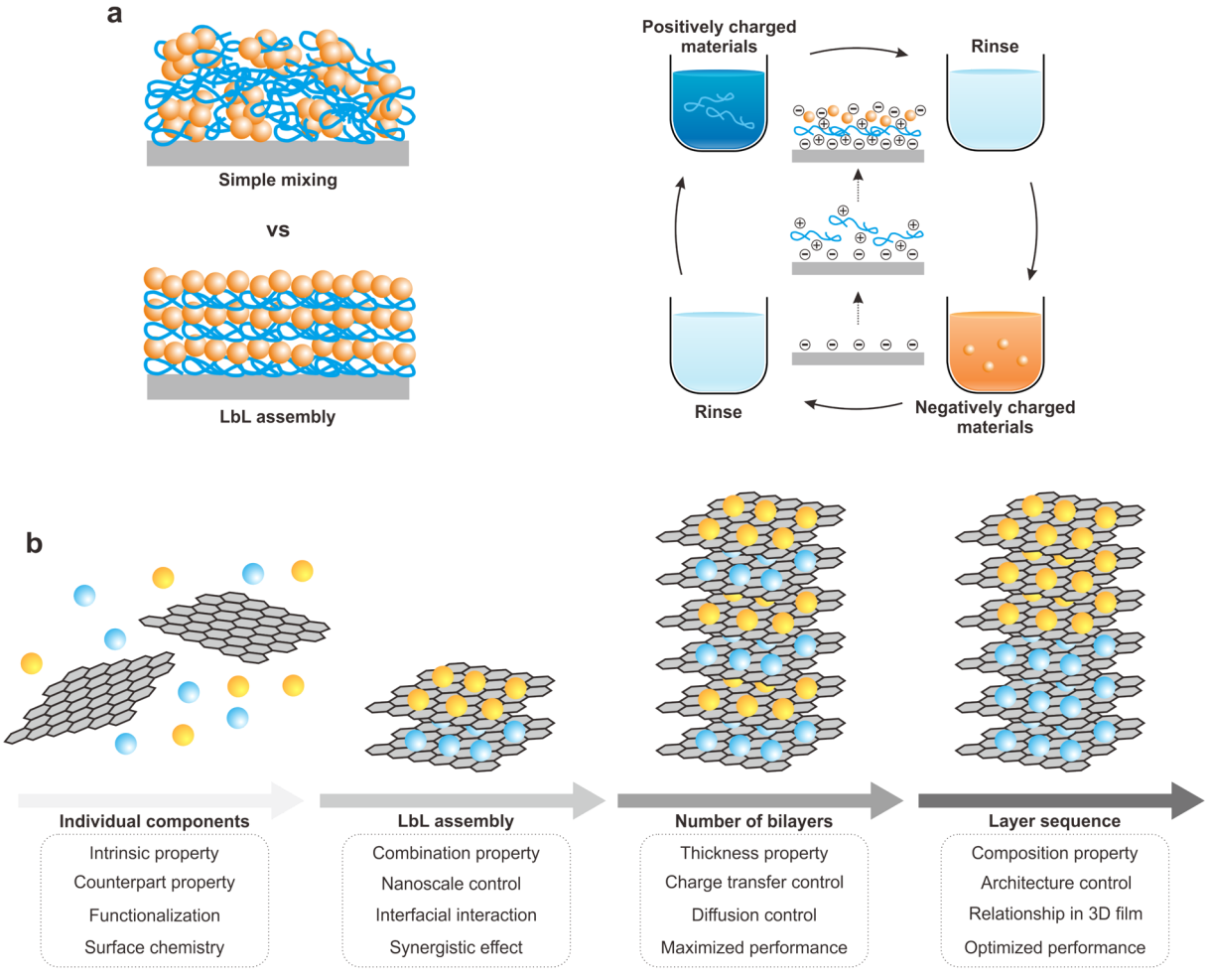


**Figure 2.** (a) Comparison of electrode fabrication methods (i.e., simple mixing vs LbL assembly) and (b) tunable properties of LbL assembled three-dimensional (3D) electrodes for electrochemical analysis.

## 1. INTRODUCTION

### 1.1. Electrochemical Surface Reactions on Electrodes

As increasing environmental concerns have increased the demand for clean energy, various technologies have been developed to utilize eco-friendly and renewable energy.[4] In particular, the development of novel electroactive materials such as electrocatalysts has garnered a great deal of interest.[5] Although Pt and Pt-based materials were long considered to



https://dx.doi.org/10.1021/acs.accounts.0c00524
Acc. Chem. Res. XXXX, XXX, XXX−XXX

be the best electrocatalysts because of their high performance and efficiency, many researchers have worked to develop alternative electrocatalysts because of the limited supply and high cost of Pt. For example, nanostructured bimetallic electrocatalysts employing an alloy and core−shell structure have been proposed to overcome sluggish catalytic reactions.[6,7] Moreover, various metal- and heteroatom-doped carbon nanomaterial composite catalysts have emerged as promising alternatives as well.[8,9]

In addition to promoting fast charge transfer kinetically, another simple strategy is to expand the catalytic surface area by fabricating porous electrodes, templating with carbon substrates, and decreasing the size of active materials to the nanoscale level.[9,10] High surface area is critical to provide high current density and capacitance by increasing the number of active sites for electrochemical surface reactions and facilitating the mass transfer of reactants inside the active layer on the electrode (Figure 1).

It is essential to consider both fast charge transfer of redox reactions and fast diffusion into porous electrodes, especially in inner-sphere electrochemical reactions such as oxygen- and hydrogen-involved electrocatalysis.[11] Simultaneously, fundamental studies on electrochemistry are critical to developing highly efficient energy conversion and storage systems because most energy devices are based on interfacial electrochemical reactions on the surface of electrodes. Thus, the efficient design of electrodes is crucial to study the specific electrochemical principles and mechanisms at play in interfacial reactions on electrode surfaces.

### 1.2. Layer-by-Layer Assembly for Electrode Fabrication

Typically, electroactive materials are fabricated into thin-film electrodes via a simple mixing and casting process.[12] However, this conventional method makes it difficult to unravel the specific electrochemical contributions of each component because of the low level of structural control afforded by the random distribution of active materials within the electrode. Layer-by-layer (LbL) assembly, on the other hand, offers a versatile method for the production of highly ordered, multilayer thin-film electrodes from a diverse array of materials with nanoscale precision (Figure 2a).[13,14] Specifically, LbL assembly allows for the fabrication of a highly organized multilayer structure with nanoscale thickness via the sequential adsorption of different components exploiting diverse complementary interactions, such as electrostatic interactions, hydrogen bonding, and other intermolecular interactions.

With advancements in LbL assembly, the hybridization of the unique electrochemical properties of active materials has opened new possibilities in electrode engineering.[15−20] Additionally, various electrochemical functionalities can be achieved via simple chemical modifications and by careful material selection for LbL electrodes.[21] Many different nanoscale building blocks of varying dimensions, including nanoparticles, polymers, carbon nanotubes, and graphene derivatives, can function as electroactive materials for thin-film electrode assembly (Figure 2b). These thin-film electrodes can be further developed into porous multilayer electrodes by increasing the number of bilayers (BLs), a key parameter in LbL assembly. Furthermore, LbL assembly allows for the verification of the internal-architecture-dependent electrochemical performance between inner and outer layers within the electrode simply by changing the layer sequence, another key parameter in LbL assembly. The specific tunable properties afforded by architecture-controlled electrodes for electrochemical analysis are summarized in Figure 2b.

### 1.3. Thin-Layer Electrochemistry in LbL Electrodes

LbL electrode performance is dictated by the material choice, film thickness, and internal architecture. In general, the current is governed by both the charge transfer kinetics and mass transfer based on linear diffusion at the large surface of a planar electrode. However, unlike the bulk electrochemical reactions on a thick film electrode, only adsorbed electroactive species are confined to surface reaction in thin-layer electrochemistry, as the film thickness, $T$, is smaller than the diffusion layer thickness (eq 1):[22]

$$T \ll \sqrt{2Dt} \tag{1}$$

where $D$ and $t$ are the diffusion coefficient ($cm^2/s$) and diffusion time (s) of the electroactive species, respectively. Thus, negligible mass transfer occurs within thin-film electrodes (Figure 3). In other words, these electrochemical LbL thin-film electrodes allow for a shift from a surface-confined process to a diffusion-limited process as a function of the number of BLs because the thickness of the LbL multilayer thin film, $T$, is tunable within a range from several nanometers to hundreds of nanometers. Because LbL multilayers are highly sensitive to the rate-limiting step of the overall electrochemical process

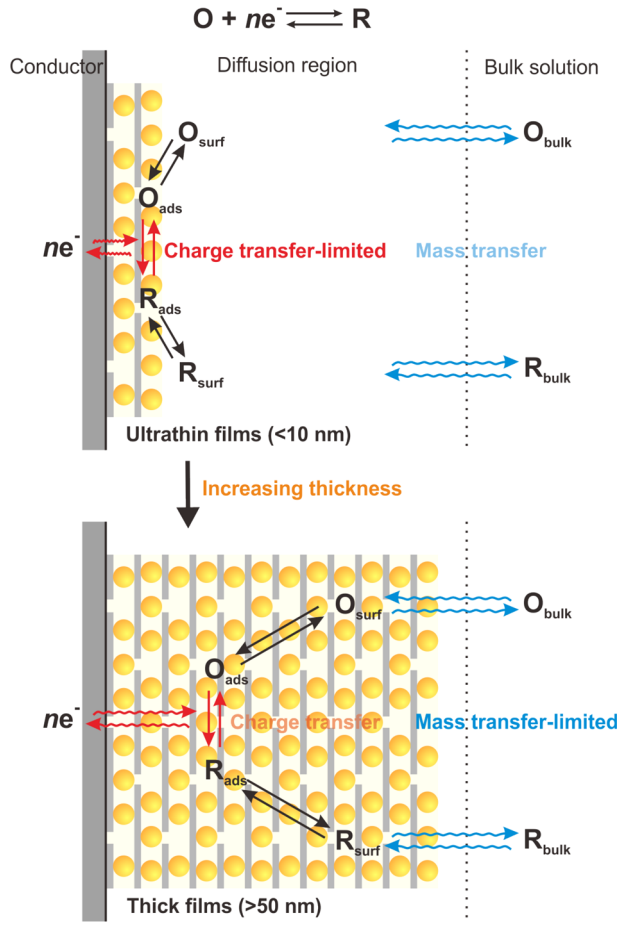


**Figure 3.** Thickness-dependent transition of electrochemical reactions based on charge and mass transfer within a thin-film electrode to a porous multilayer electrode in electrolyte. Schemes of ideally organized LbL films are presented (Figure 7 shows a representative real LbL structure under cross-sectional TEM).


https://dx.doi.org/10.1021/acs.accounts.0c00524
Acc. Chem. Res. XXXX, XXX, XXX−XXX

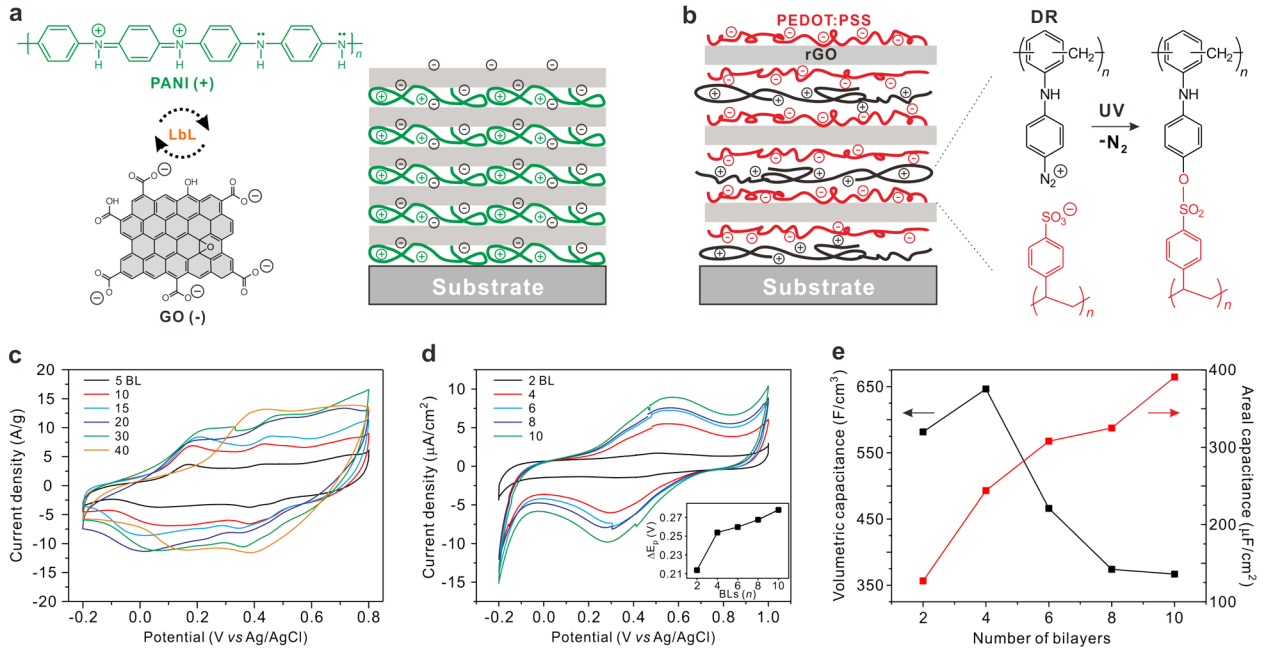


**Figure 4.** Schematic representation of (a) LbL multilayer electrodes of PANI with GO nanosheets and (b) photochemical cross-linkable LbL multilayer thin films with DR and rGO-PEDOT/PSS. (c, d) Cyclic voltammograms of (c) $(PANI/GO)_n$ ($n$ = 5−40) in 1.0 M $H_2SO_4$ at a scan rate of 10 mV/s and (d) $(DR/rGO\text{-}PEDOT:PSS)_n$ ($n$ = 2−10) in 1.0 M $H_2SO_4$ at a scan rate of 20 mV/s. The inset in (d) shows the anodic/cathodic peak-to-peak separation of $(DR/rGO\text{-}PEDOT:PSS)_n$ with respect to the number of bilayers. (e) Volumetric and areal capacitances of each layer after UV treatment. Reproduced with permission from refs 34 and 1. Copyright 2012 Royal Society of Chemistry and 2015 American Chemical Society, respectively.

occurring on the surface of the electrode, LbL assembly provides a good platform to study the mass and charge transfer system in regard to electrochemistry.

Although there are many excellent reviews in the area of nanocomposites based on LbL assembly,[14−16,23−25] most are focused on the aspect of material engineering for multilayer nanocomposites using carbon nanomaterials, polymers, and inorganic nanoparticles (NPs) for potential energy applications without detailed fundamental analysis of the relevant electrochemistry. However, these multilayer electrodes offer a unique potential platform for electrochemical mechanistic studies by controlling the kinetics and diffusion. As electrochemical LbL research has progressed over the last 10 years, our group has performed pioneering studies on the underlying fundamental electrochemical properties of multilayer electrodes fabricated via LbL assembly for diverse energy applications such as photo- and electrocatalysts,[2,3,26−33] supercapacitors,[1,34] and Li-ion batteries.[35,36] In this Account, we aim to introduce the fundamentals and applications of LbL-assembled multilayer thin-film electrodes with new insight combining materials engineering and electrochemistry. This insight will prove beneficial for the development of advanced electronic, energy, and sensor applications via the optimization of charge and mass transfer in electrodes due to the intrinsic properties of electroactive materials and the precise architecture control afforded by LbL assembly.

## 2. ELECTROCHEMICALLY ACTIVE LBL ELECTRODES

### 2.1. Layer-Dependent Electrochemistry

LbL-assembled multilayer electrodes are applicable toward a wide range of energy storage and conversion fields because of their tailorable architectures and compositions and tunable properties. Here we first introduce some examples of energy storage applications. As an early example of an electrochemical LbL multilayer electrode, Kotov et al. investigated the electrochemical properties of LbL-assembled electrodes using non-exfoliated graphite oxide platelets.[37] Furthermore, the Hammond and Shao-Horn groups demonstrated that LbL-assembled multiwalled carbon nanotube electrodes exhibit a high gravimetric energy of 200 W h $kg^{-1}$ with high capacity and electronic conductivity for Li-ion batteries.[38−40] It was demonstrated that the LbL system offers not only an opportunity to design ideal electrochemical electrodes for supercapacitors, batteries, and fuel cells but also bridges the performance gap between non-Faradaic electrical double layer capacitors and Faradaic Li-ion batteries.

In other work, the conducting polymer polyaniline (PANI) and transition metal NPs with high Faradaic capacitance were assembled with carbon nanomaterials in LbL electrodes to further improve the electrochemical performance.[40−42] The Kim and Lutkenhaus groups demonstrated these features in a combination of the pseudocapacitance of PANI with the non-Faradaic electrical double layer capacitance of graphene oxide (GO) supports, emphasizing the unique physical and electrochemical properties of two-dimensional (2D) GO nanosheets as a support for LbL electrodes (Figure 4a,c).[34,43] Interestingly, both LbL electrodes were optimized as a function of the number of BLs (i.e., the thickness). Specifically, the overall capacitance or current density initially increases with the number of BLs but then gradually decreases beyond a specific number of BLs. This observation suggests that there is an electrochemical balance between the electron transfer from redox reactions within the LbL multilayers and the ionic mass transfer from the bulk electrolyte. Similarly, this thickness-dependent electrochemical property was also observed in other LbL-assembled energy storage electrodes, including PANI/vanadium pentoxide[44,45] and aramid nanofibers/GO.[46,47]


https://dx.doi.org/10.1021/acs.accounts.0c00524
Acc. Chem. Res. XXXX, XXX, XXX−XXX

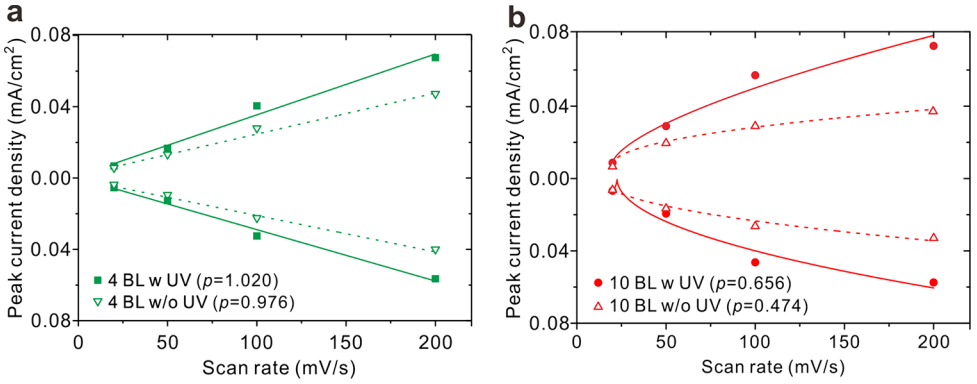


**Figure 5.** Plots of current density vs scan rate for an LbL-assembled $(DR/rGO\text{-}PEDOT:PSS)_n$ multilayer electrode at (a) four BLs and (b) 10 BLs before (dotted lines) and after (solid lines) UV treatment. Reproduced from ref 1. Copyright 2015 American Chemical Society.

We examined this distinct BL dependence by electrochemically analyzing the reversible capacitive behavior of an LbL-assembled ultrathin supercapacitor electrode using reduced graphene oxide (rGO) functionalized with a conducting polymer, poly(3,4-ethylenedioxythiophene):poly(styrenesulfonate) (PEDOT:PSS) and a photo-cross-linkable diazo resin (DR) (Figure 4b).[1] This hybrid supercapacitor electrode exhibits pseudocapacitance resulting from the reversible Faradaic reaction of PEDOT:PSS as well as electrical double layer capacitance from the rGO nanosheets. As shown in Figure 4d, the areal capacitance generally increases as the number of BLs increases because more redox-active components are deposited onto the electrodes. However, the volumetric capacitance begins to decrease after a critical thickness is reached—four BLs in this case (Figure 4e).

Prior to determining the mechanism of layer-dependent electrochemical performance in LbL electrodes, we should consider the following two systems: (1) a surface-confined system with a thin layer (typically below 10 nm) and (2) a diffusion-controlled system with a thick layer (typically above 50 nm). If the electrochemical reaction follows the Nernst equation with identical cathodic and anodic currents reversibly without any side reactions, it is regarded as thermodynamically and electrochemically reversible. In the surface-confined system with nanoscale thickness, where the mass transfer is negligible and the only adsorbed species are electrochemically active, the peak current under these conditions is given by eq 2:

$$i_p = \frac{n^2F^2\nu A\Gamma_O^*}{4RT} \tag{2}$$

where $n$ is the number of electrons transferred during the redox reaction, $F$ is the Faraday constant (C/mol), $\nu$ is the scan rate (V/s), $A$ is the area ($cm^2$), $\Gamma_O^*$ is the amount of absorbed components on the electrode surface ($mol/cm^2$), $R$ is the ideal gas constant ($J\ K^{-1}\ mol^{-1}$), and $T$ is the absolute temperature (K). In this system with an ideal Nernstian reaction, the anodic peak current ($i_{pa}$) and potential ($E_{pa}$) are identical to the cathodic peak current ($i_{pc}$) and potential ($E_{pa}$) (eq 3):

$$i_{pa} = i_{pc} \quad \text{and} \quad E_{pa} = E_{pc} \tag{3}$$

showing the mirror images of the anodic and cathodic waves. However, the anodic and cathodic peak-to-peak separation ($\Delta E_p$) of LbL-assembled $(DR/rGOPEDOT:PSS)_n$ films gradually increases as the number of BLs increases from two to 10, as shown in the inset of Figure 4d, because mass transfer becomes more critical than charge transfer as the film thickness increases. As a result, in a relatively thick multilayer electrode, the capacitive behavior shifts from a charge-transfer-limited process to a mass-transfer-limited process, and the peak current is given by eq 4:

$$i_p = (2.69 \times 10^5)n^{3/2}AD_O^{1/2}C_O^*\nu^{1/2} \tag{4}$$

where $D_O$ is the diffusion coefficient ($cm^2/s$), $C_O^*$ is the bulk concentration of redox components ($mol/cm^3$), and $\nu$ is the scan rate (V/s). According to the current equations describing surface-confined or diffusion-limited systems, the peak current is proportional to $\nu$ and $\nu^{1/2}$, respectively. Therefore, one can characterize the electrochemical processes within LbL multilayer electrodes by plotting the peak current versus the scan rate as follows (eq 5):

$$i \propto \nu^p \tag{5}$$

As shown in Figure 5, the value of $p$ changes from 1 to 0.5 as the thickness of the multilayer increases. Specifically, in this system of $(DR/rGOPEDOT:PSS)_n$ electrodes, the transition of the operating electrochemical principle from a charge-transfer-limited process to a mass-transfer-limited process occurs at four BLs, which corresponds to a thickness of 4 nm. This result demonstrates the importance of fundamental electrochemistry to LbL-assembled multilayer film electrodes.

### 2.2. Architecture-Dependent Electrochemistry

Systems based on irreversible electrochemical reactions, such as the irreversible oxidation reactions of organic molecules, can also be demonstrated with LbL electrodes. For a surface-confined system with nanoscale thickness, the peak current is given with an additional parameter, the transfer coefficient ($\alpha$), as shown in eq 6:

$$i_p = \frac{\alpha F^2A\nu\Gamma_O^*}{2.718RT} \tag{6}$$

Moreover, the peak current in diffusion-limited films is given by eq 7:

$$i_p = (2.99 \times 10^5)\alpha^{1/2}AC_O^*D_O^{1/2}\nu^{1/2} \tag{7}$$

Similar to the case of a reversible reaction, the peak current here is also proportional to $\nu$ and $\nu^{1/2}$ for surface-confined and diffusion-limited systems, respectively. Therefore, one can examine the relationship between the film thickness and the electrochemical system. Particularly, in diffusion-limited processes, controlling the mass transfer of the reactants is a more influential factor for electrocatalysis.


https://dx.doi.org/10.1021/acs.accounts.0c00524
Acc. Chem. Res. XXXX, XXX, XXX−XXX

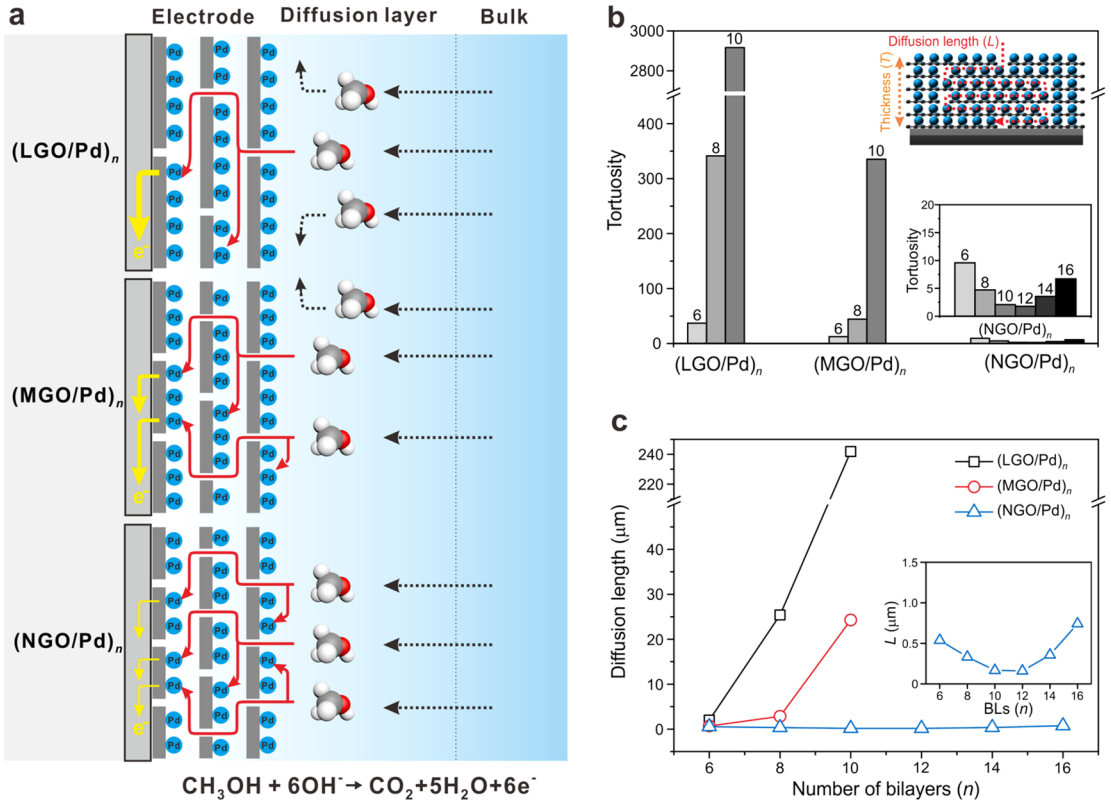


**Figure 6.** (a) Schematic representation of LbL-assembled $(GO/Pd)_n$ multilayer thin-film electrodes with varying dimensions of GO nanosheets (i.e., large-sized GO (LGO), medium-sized GO (MGO), and nanosized GO (NGO)) for the methanol oxidation reaction. (b) Calculated tortuosities and (c) diffusion lengths of methanol in $(LGO/Pd)_n$, $(MGO/Pd)_n$, and $(NGO/Pd)_n$ multilayer electrodes. Reproduced with permission from ref 27. Copyright 2018 Royal Science of Chemistry.

Thus, the effects of diffusion within LbL-assembled electrocatalytic multilayer electrodes can be investigated by controlling the porosity and internal architecture. For example, GO nanosheets were employed as electrocatalytic supports for LbL electrodes with Pd NPs for the methanol oxidation reaction, and the electrocatalytic activity was found to be highly tunable under mass transfer-limited conditions through control of the diffusion pathways of methanol by variation of the dimensions of the GO nanosheets (i.e., large-sized GO (LGO, ~50 $\mu m^2$), medium-sized GO (MGO, ~0.6 $\mu m^2$), and nanosized GO (NGO, ~0.4 × $10^{-3}$ $\mu m^2$)) (Figure 6a).[27] Because 2D GO nanosheets make tortuous diffusion pathways within the LbL electrodes, the tortuosity ($\tau$) and diffusion length ($L$) of each multilayer film can be obtained using eq 8:

$$\tau = \frac{D}{D_O} = \frac{L}{T} \tag{8}$$

where $D_O$ is the diffusion coefficient ($cm^2/s$) on a pure metal catalyst and $T$ is the film thickness (nm). Because of the much higher $D$ values of nanosized $(NGO/Pd)_n$ films compared with larger sized $(MGO/Pd)_n$ and $(LGO/Pd)_n$ films, the $\tau$ and $L$ values of $(NGO/Pd)_n$ films are significantly smaller than those of the other multilayer films in the order of NGO < MGO < LGO, as shown in Figure 6b,c, respectively. Thus, $(LGO/Pd)_n$ experiences a considerably longer tortuous path, with reactants taking a detoured diffusion into the inner catalytic surface of the films, resulting in earlier mass transfer limitations and a thinner optimized thickness than for the other films, although the charge transfer resistance of LGO is lower with this decreased thickness.

Furthermore, the internal architectures of these bimetallic electrocatalysts can be modulated by adjusting the assembly sequence of LbL films, and thus the relative positions of the Au and Pd NPs, to further investigate structure−property relationships between different LbL films with identical compositions (Figure 7a).[2] For example, in a two-component system composed of active species A and B, both compartmented structures (i.e., AABB and BBAA) and a fully alternating structure (i.e., ABAB) can be fabricated. Interestingly, we found that (i) coassembled $(GO/Au/GO/Pd)_n$ electrodes exhibit superior electrocatalytic activities via a synergistic bimetallic effect compared with monometallic $(GO/Au)_n$ and $(GO/Pd)_n$ electrodes; (ii) the electrocatalytic activity is highly tunable by adjusting which metal NPs are positioned in the inner or outer layers of the LbL structure; and (iii) it is more beneficial to generate a high concentration profile of reactants within the diffusion layer at the bottom LbL films, considering the sequence of two-step reactions facilitated by an intermediate formate species as shown in Figure 7b,c. This is the case because methanol oxidation occurs via a sequential two-step reaction depending on the type of NPs, for instance, an indirect pathway with intermediate formate produced on the surfaces of Au NPs, while Pd NPs can directly oxidize methanol to the final product, carbon dioxide. Similarly, different catalytic performance through sequential reactions within the multiple layers of redox-active enzymes was reported in the design of LbL architectures.[48]

Importantly, $i_p$ increases gradually with increasing concentrations of electroactive materials upon LbL assembly with electrochemical surface areas (ECSAs). The ECSA can be


https://dx.doi.org/10.1021/acs.accounts.0c00524
Acc. Chem. Res. XXXX, XXX, XXX−XXX

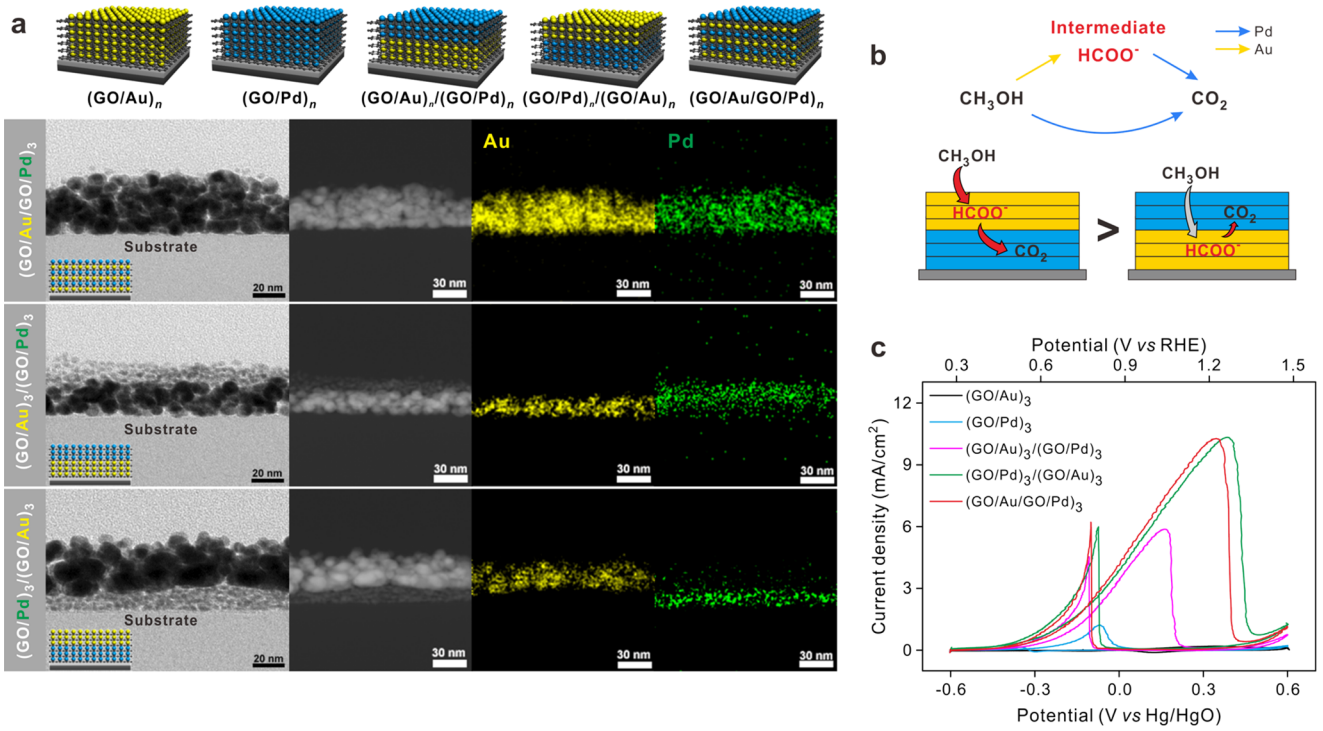


**Figure 7.** (a) Representative cross-sectional high-resolution TEM and HAADF-STEM images with composed elemental mapping images of Au (yellow) and Pd (green) NPs of architecture-controlled multilayer thin-film electrodes for the methanol oxidation reaction. Schematic representations of LbL-assembled monometallic $(GO/Au)_n$ and $(GO/Pd)_n$ and bimetallic $(GO/Au)_n/(GO/Pd)_n$, $(GO/Pd)_n/(GO/Au)_n$, and $(GO/Au/GO/Pd)_n$ multilayer electrodes are also shown. (b) Schematic reaction pathways and (c) cyclic voltammograms for the methanol oxidation reaction in architecture-controlled Au and Pd multilayer electrodes supported with graphene oxide (GO) nanosheets. Reproduced with permission from ref 2. Copyright 2016 Elsevier.

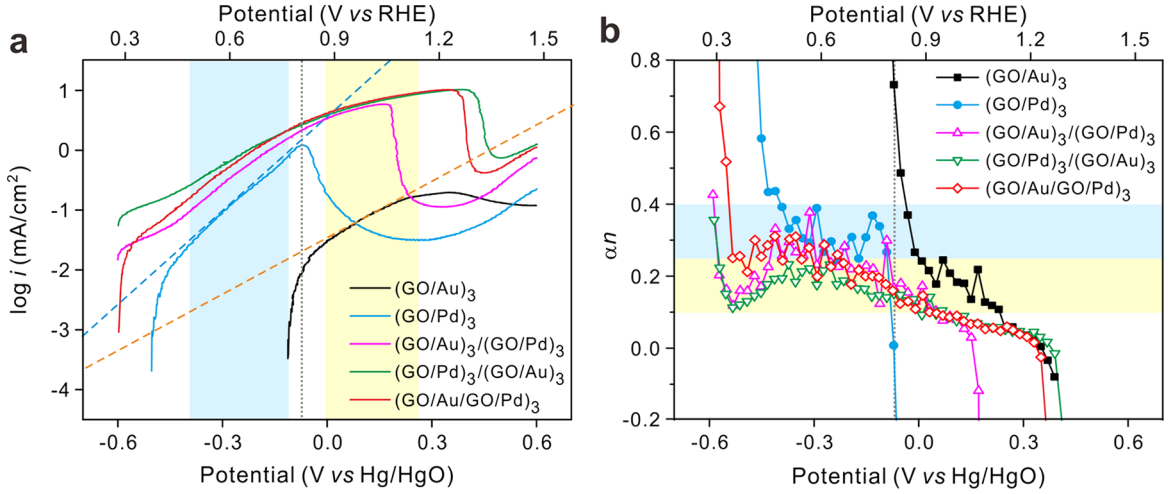


**Figure 8.** (a) Tafel plots and (b) calculated $\alpha n$ values of $(GO/Au)_n$, $(GO/Pd)_n$, $(GO/Au)_n/(GO/Pd)_n$, $(GO/Pd)_n/(GO/Au)_n$, and $(GO/Au/GO/Pd)_n$ multilayer electrodes for the methanol oxidation reaction, where $\alpha$ is the transfer coefficient and $n$ is the number of electrons. Yellow and blue areas are the charge-transfer-limited Tafel regions corresponding to $(GO/Au)_n$ and $(GO/Pd)_n$, respectively. Reproduced with permission from ref 2. Copyright 2016 Elsevier.

calculated using hydrogen underpotential deposition, carbon monoxide stripping, or the reduction peak of a metal oxide layer using eq 9:

$$\mathrm{ECSA} = \frac{\int I \, dV}{\sigma v} \tag{9}$$

where $\sigma$ is the reference charge density (e.g., $\sigma$ is 0.210, 0.424, and 0.386 mC/cm$^2$ for Pt, Pd, and Au NPs, respectively). In the internal-architecture-controlled LbL multilayer electrode, however, the ECSA values of films of identical compositions are effectively equal, indicating that enhanced catalytic performance is due to mass transfer afforded by different architectures.

In addition to enhancing diffusion of reactants into multilayer thin films, the effects of charge transfer are also crucial to investigate, as enhanced charge transfer may accelerate the electrochemical kinetics with decreased charge transfer resistance. To elucidate the kinetics of heterogeneous multilayer


https://dx.doi.org/10.1021/acs.accounts.0c00524
Acc. Chem. Res. XXXX, XXX, XXX−XXX

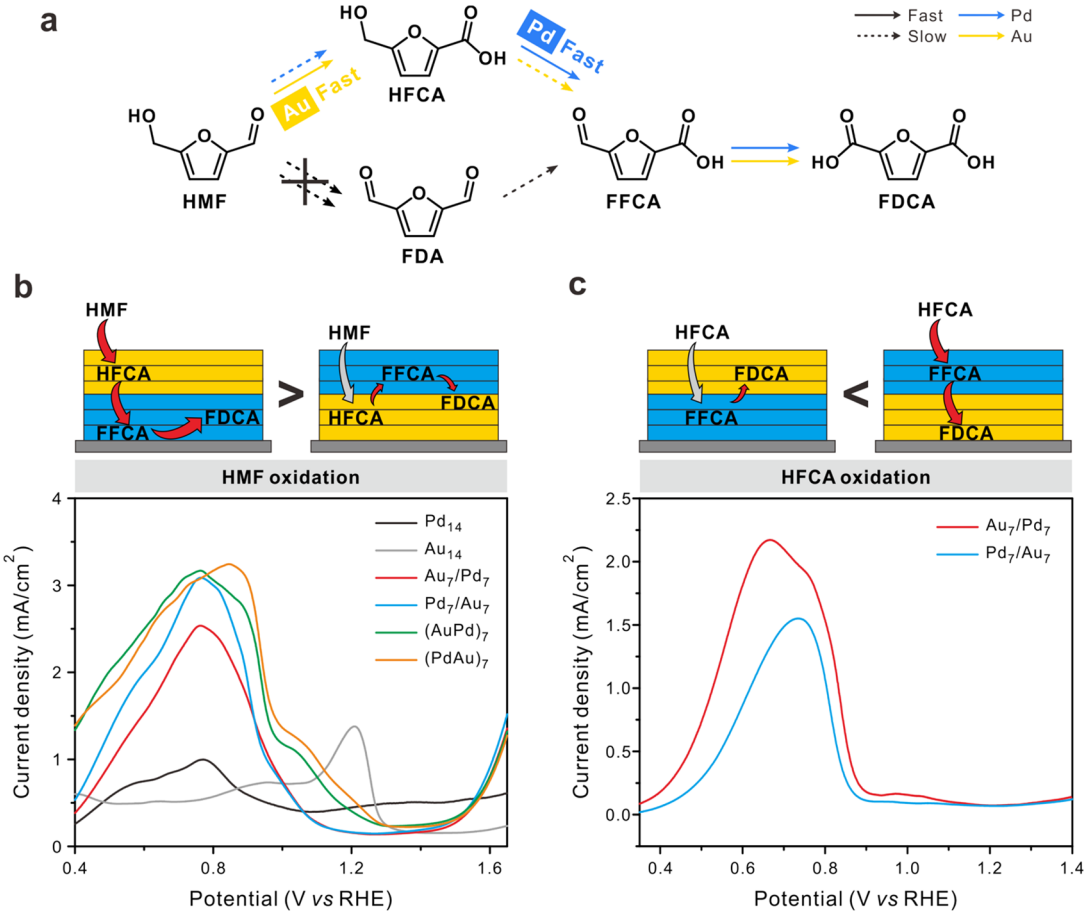


**Figure 9.** (a) Schematic reaction pathways for the sequential oxidation of 5-hydroxymethylfurfural (HMF) to 2,5-furandicarboxylic acid (FDCA) with Au and Pd NPs through various intermediates: 2,5-furandicarbaldehyde (FDA), 5-hydroxymethyl-2-furancarboxylic acid (HFCA), and 5-formyl-2-furancarboxylic acid (FFCA). (b, c) Electrocatalytic activities for the (b) HMF and (c) HFCA oxidation reactions obtained by measuring linear sweep voltammograms at a scan rate of 2.0 mV $s^{-1}$ with 10 mM HMF in a 1.0 M KOH electrolyte. The proposed reaction mechanisms using ($Pd_7/Au_7$) and ($Au_7/Pd_7$) multilayer electrodes are also shown. Reproduced from ref 3. Copyright 2020 American Chemical Society.

thin films in which mass transfer is not a determining factor for the current, the Tafel plot of each multilayer electrode was generated, as shown in Figure 8a. The current is related exponentially to the overpotential ($\eta$) by the Tafel equation, derived from the Butler–Volmer equation (eqs 10 and 11):

$$\eta = a + b \log i \tag{10}$$

$$a = \frac{\ln i_0}{\alpha n F} \quad \text{and} \quad b = -\frac{2.3}{\alpha n F} \tag{11}$$

where $\alpha$ is the transfer coefficient and $n$ is the number of electrons. Using the Tafel equation, we can obtain the exchange current ($i_0$) and the Tafel slope ($b$), which describes the electrocatalytic efficiency in the linear Tafel region with negligible mass transfer (*i.e.*, the yellow and blue Tafel regions correspond to $(GO/Au)_n$ and $(GO/Pd)_n$, respectively). A smaller Tafel slope indicates faster kinetics (e.g., 192 mV/dec for $(GO/Pd)_n$ vs 311 mV/dec for $(GO/Au)_n$). The nonlinear plot outside the Tafel region indicates that mass transfer begins to limit the electrocatalysis at high $\eta$ by overcoming the slow kinetics. Therefore, depending on which metal NPs are used in the outer layer, the kinetics of bimetallic multilayer films is determined by the competition between the mass-transfer-limited system of $(GO/Pd)_n$ and the charge-transfer limited-system of $(GO/Au)_n$ films in the overlapped potential region from 0 to 0.25 V (yellow region in Figure 8).

Furthermore, we can determine $\alpha$ and $n$ from the Tafel slope depending on the electrochemical system. For example, the specific number of electrons, $n$, can be obtained by applying $\alpha$ = 0.5 in the case of reversible and multiple charge transfer rate-determining reactions (e.g., the oxygen reduction reaction).[49] On the other hand, in the case of the irreversible methanol oxidation reaction, the specific $\alpha$ can be obtained by assuming $n$ = 1 because the first charge transfer is the rate-determining step for the dissociation of methanol by C–H bond breaking. By plotting $\alpha n$ versus the potential as shown in Figure 8b, we confirmed the asymmetry of the energy barrier for the irreversible methanol oxidation reaction below $\alpha$ = 0.5. Furthermore, the kinetics of bimetallic electrodes is highly affected by the competitive mass and charge transfer relationship between Pd and Au NPs in the Tafel range with $\alpha$ values between 0 and 1.

Most recently, we demonstrated that these architecture-controlled bimetallic electrodes can also modulate more complex electrocatalysis with multistep sequential reactions such as the 5-hydroxymethylfurfural (HMF) oxidation reaction (Figure 9a).[3] Although there are three reaction steps with two possible pathways to produce the final product, 2,5-furandicarboxylic acid (FDCA), through various intermediates of different oxidation levels, the current density of Au NPs located in the outer layer of the electrode (i.e., ($Pd_7/Au_7$)) is higher than


https://dx.doi.org/10.1021/acs.accounts.0c00524
Acc. Chem. Res. XXXX, XXX, XXX–XXX

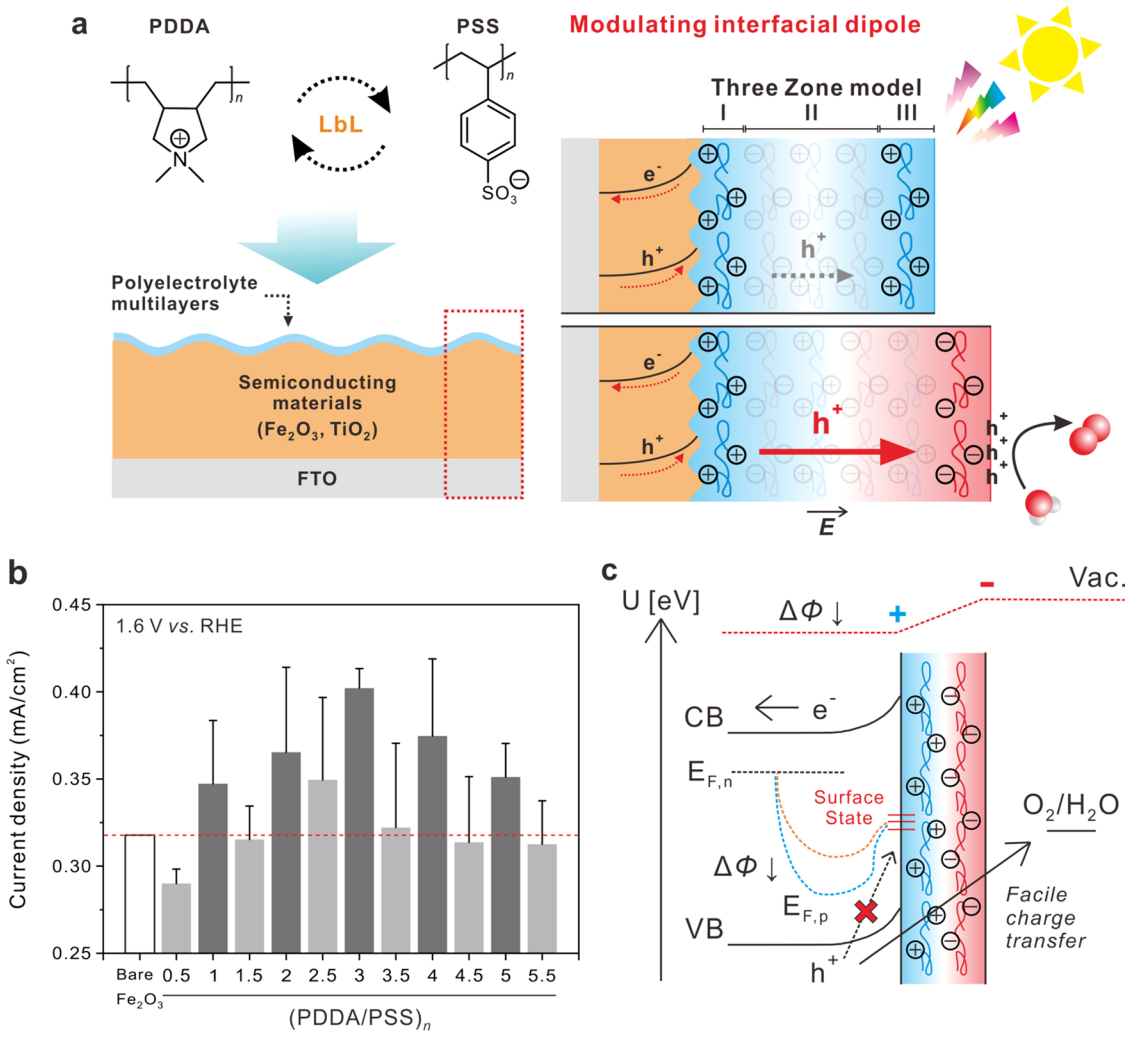


**Figure 10.** (a) Schematic illustrations of LbL-assembled polyelectrolyte multilayers (PEMs) to modulate the interfacial dipole on photoelectrodes for the oxygen evolution reaction. (b) Current density vs the number of BLs and types of terminal polyelectrolytes on $Fe_2O_3$ photoanodes. The PEMs with negative terminal charge (i.e., PSS as the terminal layer) are denoted by integers, and those with positive terminal charge (i.e., PDDA as the terminal layer) by decimal numbers. (c) Schematic representation showing the improved charge separation efficiency of photoanodes after deposition of PEM films. Reproduced with permission from ref 31. Copyright 2019 Wiley-VCH.

that of Au NPs located in the inner layer of the electrode (i.e., $(Au_7/Pd_7)$) (Figure 9b) because Au NPs favor the first-step conversion of HMF into 5-hydroxymethyl-2-furancarboxylic acid (HFCA). The generated HFCA is subsequently supplied as a reactant to inner-layer Pd NPs to facilitate the conversion toward the final product, FDCA, affording a high concentration profile of reactants that enhances the mass transfer for the 3D multilayer electrodes. In contrast, the electrocatalytic performance of $(Au_7/Pd_7)$ electrodes for converting the first intermediate, HFCA, to FDCA is higher than that of $(Pd_7/Au_7)$ electrodes (Figure 9c) because Pd NPs rapidly oxidize HFCA to the second intermediate, 5-formyl-2-furancarboxylic acid (FFCA). These differences in electrocatalytic performance and product distribution clearly demonstrate that sequential electrochemical reaction pathways are highly dependent on the choice of catalyst and the architecture of the 3D multilayer electrodes.

## 3. ELECTROCHEMICALLY INACTIVE LBL ELECTRODES

### 3.1. Interfacial Dipole Layers

When electroactive components are assembled into multilayer electrodes via LbL assembly, the resulting thin films are themselves electroactive, and redox reactions occur within the structures. In contrast, when LbL films are assembled with electrochemically inert polymers, the electrochemical reactions of the underlying semiconducting electrodes can be tailored. For this purpose, conventional polyelectrolytes for LbL assembly were employed, including poly(diallyldimethylammonium chloride) (PDDA) and poly(styrenesulfonate) (PSS). Importantly, these polyelectrolytes do not exhibit Faradic current or catalytic effects.

Interestingly, the deposition of polyelectrolyte multilayers (PEMs) of cationic PDDA and anionic PSS on the surface of photocatalytic electrodes modulates the charge separation efficiency by inducing the formation of interfacial dipole layers (Figure 10a).[31] The passivation effect of defect sites and the interface dipole due to the polyelectrolyte layers have previously been reported in polymer-based light-emitting diodes and solar cells.[50] Because of the versatility afforded by LbL assembly, PEM


https://dx.doi.org/10.1021/acs.accounts.0c00524
Acc. Chem. Res. XXXX, XXX, XXX−XXX

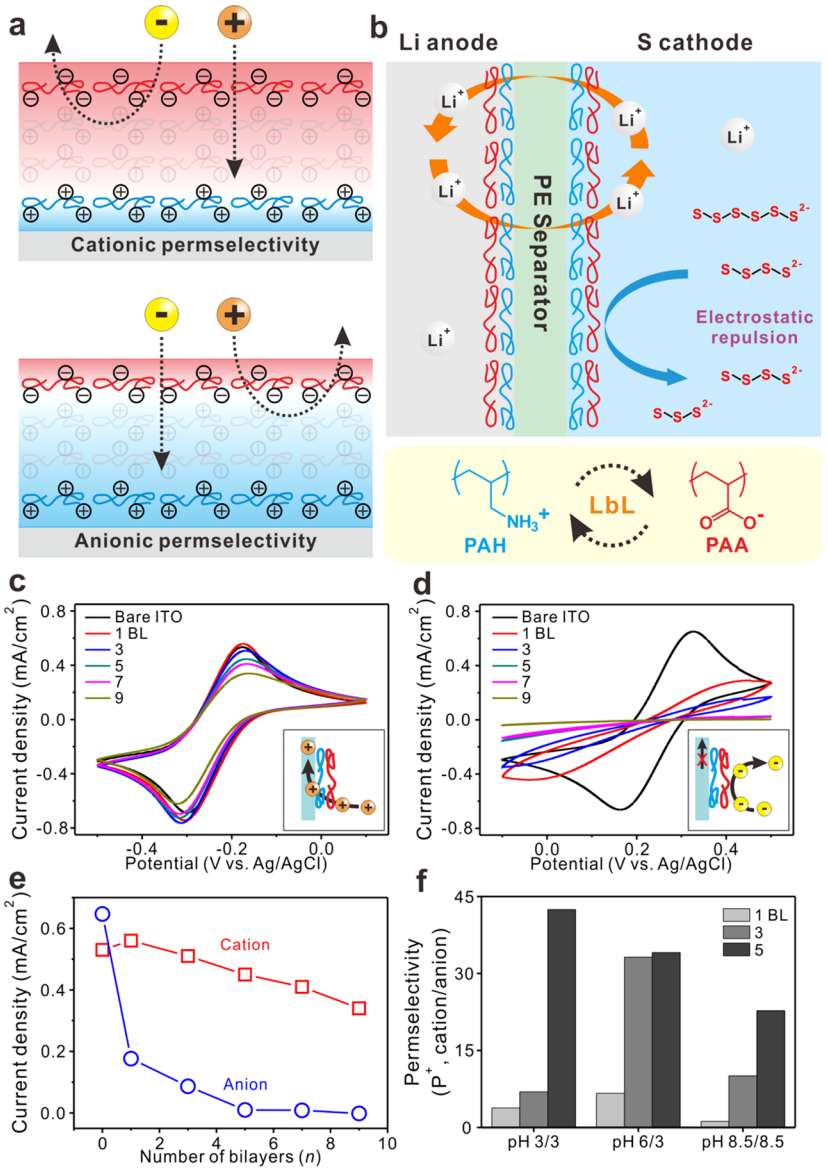


**Figure 11.** Schematic representations of (a) cationic and anionic permselective LbL thin-film-coated electrodes and (b) ion-permselective $(PAH/PAA)_n$ multilayer films for inhibiting the shuttle effect of polysulfide across the polyethylene separator in a Li−S battery. (c, d) Cyclic voltammograms of $(PAH/PAA)_n$ multilayers of pH 3/3 coated on indium tin oxide (ITO) glass by LbL assembly in an aqueous 0.50 M $Na_2SO_4$ electrolyte solution containing 5.0 mM (c) $Ru(NH_3)_6^{3+}$ as a cationic probe and (d) $Fe(CN)_6^{3-}$ as an anionic probe. The inset images show schematic representations of the cation exchange properties of the LbL thin films. (e) Anodic peak current density for each ion species. (f) Calculated cationic permselectivity ($P^+$) (selectivity ratio of cation to anion) with varying numbers of BLs and pH conditions. Reproduced with permission from ref 35. Copyright 2014 Royal Society of Chemistry.

films not only tune the magnitude of interfacial dipole moments by control of the film thickness but also tailor the direction by switching of the terminal polyelectrolyte layer. For instance, PEM films terminated with PSS starting from cationic PDDA used in the first layer (i.e., $(PDDA/PSS)_n$) exhibit a higher photocurrent density than those terminated with PDDA (i.e., $(PDDA/PSS)_nPDDA$) (Figure 10b). In addition, the highest current density was obtained at three BLs, evidencing the thickness-dependent performance of LbL electrodes as previously discussed. This is due to the optimized potential gradient and shifted flat-band potential, which improve the charge separation efficiency of generated electron−hole pairs over the photocatalytic electrode (Figure 10c).

### 3.2. Ion-Permselective Layers

LbL-assembled weak PEM thin films composed of poly(amine hydrochloride) (PAH) and poly(acrylic acid) (PAA) demonstrate ion-permselective properties (Figure 11a). In general, anionic or cationic permselectivity of bipolar LbL films can be controlled by variation of the pH of the film assembly and the pH of the bulk electrolyte during electrochemical measurements.[51] This ion selectivity can be practically applied to inhibit the shuttle effect of polysulfide across the separator in Li−S batteries (Figure 11b).[35] We evaluated the ion-selectivity using two oppositely charged redox probe molecules, namely, cationic $Ru(NH_3)_6^{3+}$ (Figure 11c) and anionic $Fe(CN)_6^{3-}$ (Figure 11d). Although one-electron redox reactions of both $Ru(NH_3)_6^{3+}$ and $Fe(CN)_6^{3-}$ are outer-sphere electrochemical reactions, electron tunneling was effectively blocked with a 72% decrease in current


https://dx.doi.org/10.1021/acs.accounts.0c00524
Acc. Chem. Res. XXXX, XXX, XXX−XXX

density even with one BL (Figure 11e). Interestingly, the anionic $Fe(CN)_6^{3-}$ was significantly inhibited by the $(PAH/PAA)_n$ films (i.e., decreasing current density with increasing number of BLs), while the current density using cationic $Ru(NH_3)_6^{3+}$ decreased by only 15% at five BLs because of the physically limited diffusion of $Ru(NH_3)_6^{3+}$. This indicates that only cationic $Ru(NH_3)_6^{3+}$ probes can penetrate though the LbL PEM films to the ITO surfaces, which act as a cation-exchange membrane. This is the case because when electrochemical measurements are conducted on the $(PAH/PAA)_n$ film-coated electrodes in a neutral solution above the $pK_a$ value of PAA (~5), a significant fraction of free carboxylic acid groups of PAA adsorbed on fully ionized PAH are deprotonated to form anionic carboxylate groups. As a result, the negative internal charge density induced by the carboxylate groups of the $(PAH/PAA)_n$ films can repel anionic $Fe(CN)_6^{3-}$ probes. Similarly, when the weak polyelectrolyte PAH with $pK_a$ value of ~9 is used, anion-exchange membranes can be fabricated by controlling the positive internal charge density of ammonium ions.

The cationic permselectivity ($P^+$) or anionic permselectivity ($P^-$) can be also evaluated under different pH and thickness conditions by dividing the cationic retention ($I^+/I_o^+$) by the anionic retention ($I^-/I_o^-$) or vice versa (eq 12):

$$P^+ = \frac{I^+/I_0^+}{I^-/I_0^-} \quad \text{or} \quad P^- = \frac{I^-/I_0^-}{I^+/I_0^+} \tag{12}$$

where $I^+$ is the current density under the given condition, $I_0^+$ is the current density on a bare electrode for cation, $I^-$ is the current density under the given condition, and $I_0^-$ is the current density on a bare electrode for anion. As a result, the cationic permselectivity of $(PAH/PAA)_n$ films increases with increasing number of BLs and free carboxylic acid groups in the order of pH 3 > 6 > 8.5 (Figure 11f). This cation-permselective property of LbL multilayer thin films was similarly observed in other studies using GO-nanosheet-based multilayer films.[52,53]

## 4. SUMMARY AND OUTLOOK

In this Account, we have presented an electrochemical perspective on thickness- and architecture-controlled LbL multilayer electrodes with principles and applications. Because of the versatility of nanoscale-architecture-controllable LbL assembly compared with other electrode fabrication methods, the transition from a surface-confined process to a diffusion-controlled process can be achieved by increasing the thickness of thin-layer electrodes from 2D ultrathin films to 3D thick porous films. In addition, precisely controlled internal architecture is achieved simply by changing the order of the layer sequence, verifying the effect of diffusion in 3D multilayer electrodes under mass transfer control. In the case of electrocatalytic reactions consisting of multiple steps, it is important to consider the sequence of steps to achieve high catalytic performance. It is beneficial for the first step of the reaction to occur on the outer layer near the electrolyte, which results in enhanced mass transfer to the second step occurring in inner layers. In addition, control of the internal charge density of LbL thin films can significantly affect the overall performance by modulating the interfacial dipole as well as the ion permeability. Even though specific kinetic analysis of LbL electrodes is still required to determine the factors affecting electrochemical parameters such as the kinetic current and rate constant under charge transfer control, we envision that the LbL approach will emerge as an attractive electrochemical platform to study fundamental electrochemistry with tailored functionalities for the design and fabrication of diverse hybrid nanocomposites and future energy applications.

## AUTHOR INFORMATION


### Corresponding Author

**Byeong-Su Kim** − *Department of Chemistry, Yonsei University, Seoul 03722, Republic of Korea;* orcid.org/0000-0002-6419-3054; Email: bskim19@yonsei.ac.kr

### Author

**Minsu Gu** − *Department of Chemistry, Yonsei University, Seoul 03722, Republic of Korea; Department of Chemistry, The University of Texas at Austin, Austin, Texas 78712, United States;* orcid.org/0000-0002-6270-7496

Complete contact information is available at: https://pubs.acs.org/10.1021/acs.accounts.0c00524


### Notes

The authors declare no competing financial interest.

### Biographies

**Minsu Gu** received his B.S. from the School of Nano-Bioscience and Chemical Engineering at Ulsan National Institute of Science and Technology (UNIST), Republic of Korea, in 2013 and his Ph.D. from the Department of Energy Engineering at UNIST in 2018 under the supervision of Prof. Byeong-Su Kim. He is now a postdoctoral researcher in Dr. Allen J. Bard's group in the Department of Chemistry at the University of Texas at Austin. His research interest is electrochemistry of functional nanomaterials and polymers for energy conversion and storage applications.

**Byeong-Su Kim** is an Associate Professor in the Department of Chemistry at Yonsei University, Republic of Korea. He received his B.S. and M.S. in Chemistry at Seoul National University and his Ph.D. in Chemistry at the University of Minnesota, Twin Cities in 2007. After his postdoctoral research in Prof. Hammond's group at MIT, he started his independent career at UNIST in 2009 and recently moved to Yonsei University in 2018. His group investigates a broad range of topics in macromolecular chemistry for the study of novel polymer and hybrid nanomaterials, including the molecular design and synthesis of self-assembled polymers and layer-by-layer assembly of functional thin films.

## ACKNOWLEDGMENTS

This work was supported by the National Research Foundation of Korea (NRF-2017M3A7B4052802, NRF-2017R1A2B3012148, and NRF-2018R1A5A1025208).

## REFERENCES


(1) Jo, K.; Gu, M.; Kim, B. S. Ultrathin Supercapacitor Electrode Based on Reduced Graphene Oxide Nanosheets Assembled with Photo-Cross-Linkable Polymer: Conversion of Electrochemical Kinetics in Ultrathin Films. *Chem. Mater.* **2015**, *27*, 7982−7989.

(2) Gu, M.; Kim, B. S. Unraveling the Importance of Controlled Architecture in Bimetallic Multilayer Electrode Toward Efficient Electrocatalyst. *Nano Energy* **2016**, *30*, 658−666.

(3) Park, M.; Gu, M.; Kim, B. S. Tailorable Electrocatalytic 5-Hydroxymethylfurfural Oxidation and $H_2$ Production: Architecture-Performance Relationship in Bifunctional Multilayer Electrodes. *ACS Nano* **2020**, *14*, 6812−6822.

(4) Turner, J. A. A Realizable Renewable Energy Future. *Science* **1999**, *285*, 687−689.




https://dx.doi.org/10.1021/acs.accounts.0c00524
*Acc. Chem. Res.* XXXX, XXX, XXX−XXX

(5) Debe, M. K. Electrocatalyst Approaches and Challenges for Automotive Fuel Cells. *Nature* **2012**, *486*, 43−51.
(6) Bing, Y. H.; Liu, H. S.; Zhang, L.; Ghosh, D.; Zhang, J. J. Nanostructured Pt-Alloy Electrocatalysts for PEM Fuel Cell Oxygen Reduction Reaction. *Chem. Soc. Rev.* **2010**, *39*, 2184−2202.
(7) Shao, M. H.; Chang, Q. W.; Dodelet, J. P.; Chenitz, R. Recent Advances in Electrocatalysts for Oxygen Reduction Reaction. *Chem. Rev.* **2016**, *116*, 3594−3657.
(8) Li, J. Y.; Zhang, M. K.; Zang, H.; Yu, B. Z.; Ma, Y. Y.; Qu, Y. Q. Chemical Doped Ternary and Quaternary Transition-Metal-Based Electrocatalysts for Hydrogen Evolution Reaction. *ChemCatChem* **2019**, *11*, 4998−5012.
(9) Liu, X.; Dai, L. Carbon-Based Metal-Free Catalysts. *Nat. Rev. Mater.* **2016**, *1*, 16064.
(10) Yang, L.; Zeng, X. F.; Wang, W. C.; Cao, D. P. Recent Progress in MOF-Derived, Heteroatom-Doped Porous Carbons as Highly Efficient Electrocatalysts for Oxygen Reduction Reaction in Fuel Cells. *Adv. Funct. Mater.* **2018**, *28*, 1704537.
(11) Bard, A. J. Inner-Sphere Heterogeneous Electrode Reactions. Electrocatalysis and Photocatalysis: The Challenge. *J. Am. Chem. Soc.* **2010**, *132*, 7559−7567.
(12) Ahmad, R.; Wolfbeis, O. S.; Hahn, Y. B.; Alshareef, H. N.; Torsi, L.; Salama, K. N. Deposition of Nanomaterials: A Crucial Step in Biosensor Fabrication. *Mater. Today Commun.* **2018**, *17*, 289−321.
(13) Decher, G. Fuzzy Nanoassemblies: Toward Layered Polymeric Multicomposites. *Science* **1997**, *277*, 1232−1237.
(14) Richardson, J. J.; Bjornmalm, M.; Caruso, F. Technology-Driven Layer-by-Layer Assembly of Nanofilms. *Science* **2015**, *348*, aaa2491.
(15) Lee, T.; Min, S. H.; Gu, M.; Jung, Y. K.; Lee, W.; Lee, J. U.; Seong, D. G.; Kim, B. S. Layer-by-Layer Assembly for Graphene-Based Multi layer Nanocomposites: Synthesis and Applications. *Chem. Mater.* **2015**, *27*, 3785−3796.
(16) Rydzek, G.; Ji, Q. M.; Li, M.; Schaaf, P.; Hill, J. P.; Boulmedais, F.; Ariga, K. Electrochemical Nanoarchitectonics and Layer-by-Layer Assembly: From Basics to Future. *Nano Today* **2015**, *10*, 138−167.
(17) Kwon, C. H.; Ko, Y.; Shin, D.; Kwon, M.; Park, J.; Bae, W. K.; Lee, S. W.; Cho, J. High-Power Hybrid Biofuel Cells using Layer-by-Layer Assembled Glucose Oxidase-Coated Metallic Cotton Fibers. *Nat. Commun.* **2018**, *9*, 4479.
(18) Michel, M.; Taylor, A.; Sekol, R.; Podsiadlo, P.; Ho, P.; Kotov, N.; Thompson, L. High-Performance Nanostructured Membrane Electrode, Assemblies for Fuel Cells made by Layer-by-Layer Assembly of Carbon Nanocolloids. *Adv. Mater.* **2007**, *19*, 3859−3864.
(19) Tung, S. O.; Ho, S.; Yang, M.; Zhang, R. L.; Kotov, N. A. A Dendrite-Suppressing Composite Ion Conductor from Aramid Nanofibres. *Nat. Commun.* **2015**, *6*, 6152.
(20) Mo, R. W.; Tung, S. O.; Lei, Z. Y.; Zhao, G. Y.; Sun, K. N.; Kotov, N. A. Pushing the Limits: 3D Layer-by-Layer-Assembled Composites for Cathodes with 160 C Discharge Rates. *ACS Nano* **2015**, *9*, 5009−5017.
(21) Ahn, E.; Lee, T.; Gu, M.; Park, M.; Min, S. H.; Kim, B.-S. Layer-by-Layer Assembly for Graphene-Based Multilayer Nanocomposites: The Field Manual. *Chem. Mater.* **2017**, *29*, 69−79.
(22) Bard, A. J.; Faulkner, L. R. *Electrochemical Methods: Fundamentals and Applications*, 2nd ed.; John Wiley & Sons: New York, 2001.
(23) Srivastava, S.; Kotov, N. A. Composite Layer-by-Layer (LBL) Assembly with Inorganic Nanoparticles and Nanowires. *Acc. Chem. Res.* **2008**, *41*, 1831−1841.
(24) Yang, M.; Hou, Y.; Kotov, N. A. Graphene-Based Multilayers: Critical Evaluation of Materials Assembly Techniques. *Nano Today* **2012**, *7*, 430−447.
(25) Lipton, J.; Weng, G. M.; Röhr, J. A.; Wang, H.; Taylor, A. D. Layer-by-Layer Assembly of Two-Dimensional Materials: Meticulous Control on the Nanoscale. *Matter* **2020**, *2*, 1148−1165.
(26) Choi, Y.; Gu, M.; Park, J.; Song, H. K.; Kim, B. S. Graphene Multilayer Supported Gold Nanoparticles for Efficient Electrocatalysts Toward Methanol Oxidation. *Adv. Energy Mater.* **2012**, *2*, 1510−1518.
(27) Gu, M.; Choi, J.; Lee, T.; Park, M.; Shin, I. S.; Hong, J.; Lee, H. W.; Kim, B. S. Diffusion Controlled Multilayer Electrocatalysts via Graphene Oxide Nanosheets of Varying Sizes. *Nanoscale* **2018**, *10*, 16159−16168.
(28) Ahn, E.; Kim, B. S. Multidimensional Thin Film Hybrid Electrodes with $MoS_2$ Multilayer for Electrocatalytic Hydrogen Evolution Reaction. *ACS Appl. Mater. Interfaces* **2017**, *9*, 8688−8695.
(29) Jeon, D.; Kim, H.; Lee, C.; Han, Y.; Gu, M.; Kim, B. S.; Ryu, J. Layer-by-Layer Assembly of Polyoxometalates for Photoelectrochemical (PEC) Water Splitting: Toward Modular PEC Devices. *ACS Appl. Mater. Interfaces* **2017**, *9*, 40151−40161.
(30) Choi, Y.; Jeon, D.; Choi, Y.; Kim, D.; Kim, N.; Gu, M.; Bae, S.; Lee, T.; Lee, H. W.; Kim, B. S.; Ryu, J. Interface Engineering of Hematite with Nacre-like Catalytic Multilayers for Solar Water Oxidation. *ACS Nano* **2019**, *13*, 467−475.
(31) Bae, S.; Kim, D.; Kim, H.; Gu, M.; Ryu, J.; Kim, B. S. Modulating Charge Separation Efficiency of Water Oxidation Photoanodes with Polyelectrolyte-Assembled Interfacial Dipole Layers. *Adv. Funct. Mater.* **2020**, *30*, 1908492.
(32) Kim, D.; Gu, M.; Choi, Y.; Kim, H.; Ryu, J.; Kim, B.-S. Bifunctional Water Splitting Photoelectrocatalysts Using Flexible Organometallic Complex and Nanographene Multilayer Thin Films. *ACS Appl. Energy Mater.* **2020**, *3*, 7103−7112.
(33) Kim, D.; Gu, M.; Park, M.; Kim, T.; Kim, B. S. Layer-by-Layer Assembly for Photoelectrochemical Nanoarchitectonics. *Mol. Syst. Des. Eng.* **2019**, *4*, 65−77.
(34) Lee, T.; Yun, T.; Park, B.; Sharma, B.; Song, H. K.; Kim, B. S. Hybrid Multilayer Thin Film Supercapacitor of Graphene Nanosheets with Polyaniline: Importance of Establishing Intimate Electronic Contact Through Nanoscale Blending. *J. Mater. Chem.* **2012**, *22*, 21092−21099.
(35) Gu, M.; Lee, J.; Kim, Y.; Kim, J. S.; Jang, B. Y.; Lee, K. T.; Kim, B. S. Inhibiting the Shuttle Effect in Lithium-Sulfur Batteries Using a Layer-by-Layer Assembled Ion-Permselective Separator. *RSC Adv.* **2014**, *4*, 46940−46946.
(36) Gu, M.; Song, W. J.; Hong, J.; Kim, S. Y.; Shin, T. J.; Kotov, N. A.; Park, S.; Kim, B. S. Stretchable Batteries with Gradient Multilayer Conductors. *Sci. Adv.* **2019**, *5*, eaaw1879.
(37) Kotov, N. A.; Dekany, I.; Fendler, J. H. Ultrathin Graphite Oxide-Polyelectrolyte Composites Prepared by Self-Assembly: Transition between Conductive and Non-Conductive States. *Adv. Mater.* **1996**, *8*, 637−641.
(38) Lee, S. W.; Kim, B. S.; Chen, S.; Shao-Horn, Y.; Hammond, P. T. Layer-by-Layer Assembly of All Carbon Nanotube Ultrathin Films for Electrochemical Applications. *J. Am. Chem. Soc.* **2009**, *131*, 671−679.
(39) Lee, S. W.; Yabuuchi, N.; Gallant, B. M.; Chen, S.; Kim, B. S.; Hammond, P. T.; Shao-Horn, Y. High-Power Lithium Batteries from Functionalized Carbon-Nanotube Electrodes. *Nat. Nanotechnol.* **2010**, *5*, 531−537.
(40) Lee, S. W.; Gallant, B. M.; Byon, H. R.; Hammond, P. T.; Shao-Horn, Y. Nanostructured Carbon-Based Electrodes: Bridging the Gap Between Thin-Film Lithium-Ion Batteries and Electrochemical Capacitors. *Energy Environ. Sci.* **2011**, *4*, 1972−1985.
(41) Hyder, M. N.; Lee, S. W.; Cebeci, F. C.; Schmidt, D. J.; Shao-Horn, Y.; Hammond, P. T. Layer-by-Layer Assembled Polyaniline Nanofiber/Multiwall Carbon Nanotube Thin Film Electrodes for High-Power and High-Energy Storage Applications. *ACS Nano* **2011**, *5*, 8552−8561.
(42) Lee, S. W.; Kim, J.; Chen, S.; Hammond, P. T.; Shao-Horn, Y. Carbon Nanotube/Manganese Oxide Ultrathin Film Electrodes for Electrochemical Capacitors. *ACS Nano* **2010**, *4*, 3889−3896.
(43) Jeon, J. W.; Kwon, S. R.; Lutkenhaus, J. L. Polyaniline Nanofiber/Electrochemically Reduced Graphene Oxide Layer-by-Layer Electrodes for Electrochemical Energy Storage. *J. Mater. Chem. A* **2015**, *3*, 3757−3767.
(44) Shao, L.; Jeon, J. W.; Lutkenhaus, J. L. Polyaniline Nanofiber/Vanadium Pentoxide Sprayed Layer-by-Layer Electrodes for Energy Storage. *J. Mater. Chem. A* **2014**, *2*, 14421−14428.
(45) Shao, L.; Jeon, J. W.; Lutkenhaus, J. L. Polyaniline/Vanadium Pentoxide Layer-by-Layer Electrodes for Energy Storage. *Chem. Mater.* **2012**, *24*, 181−189.


https://dx.doi.org/10.1021/acs.accounts.0c00524
*Acc. Chem. Res.* XXXX, XXX, XXX−XXX

(46) Park, B.; Lee, W.; Lee, E.; Min, S. H.; Kim, B. S. Highly Tunable Interfacial Adhesion of Glass Fiber by Hybrid Multilayers of Graphene Oxide and Aramid Nanofiber. *ACS Appl. Mater. Interfaces* **2015**, *7*, 3329−3334.
(47) Kwon, S. R.; Elinski, M. B.; Batteas, J. D.; Lutkenhaus, J. L. Robust and Flexible Aramid Nanofiber/Graphene Layer-by-Layer Electrodes. *ACS Appl. Mater. Interfaces* **2017**, *9*, 17125−17135.
(48) Onda, M.; Lvov, Y.; Ariga, K.; Kunitake, T. Sequential Actions of Glucose Oxidase and Peroxidase in Molecular Films Assembled by Layer-by-Layer Alternate Adsorption. *Biotechnol. Bioeng.* **1996**, *51*, 163−167.
(49) Lee, D. G.; Gwon, O.; Park, H. S.; Kim, S. H.; Yang, J.; Kwak, S. K.; Kim, G.; Song, H. K. Conductivity-Dependent Completion of Oxygen Reduction on Oxide Catalysts. *Angew. Chem., Int. Ed.* **2015**, *54*, 15730−15733.
(50) Lee, S.; Kim, D. B.; Yu, J. C.; Jang, C. H.; Park, J. H.; Lee, B. R.; Song, M. H. Versatile Defect Passivation Methods for Metal Halide Perovskite Materials and their Application to Light-Emitting Devices. *Adv. Mater.* **2019**, *31*, 1805244.
(51) Park, M. K.; Deng, S. X.; Advincula, R. C. pH-Sensitive Bipolar Ion-Permselective Ultrathin Films. *J. Am. Chem. Soc.* **2004**, *126*, 13723−13731.
(52) Ahn, E.; Gaiji, H.; Kim, T.; Abderrabba, M.; Lee, H. W.; Kim, B. S. Graphene Oxide Nanosheet as a Two-Dimensional Polyelectrolyte: pH-Responsive Behavior of a Multilayered Nanomembrane. *J. Membr. Sci.* **2019**, *585*, 191−198.
(53) Lee, T.; Kim, B. S. Two-Dimensional Designer Nanochannels for Controllable Ion Transport in Graphene Oxide Nanomembranes with Tunable Sheet Dimensions. *ACS Appl. Mater. Interfaces* **2020**, *12*, 13116−13126.


https://dx.doi.org/10.1021/acs.accounts.0c00524
*Acc. Chem. Res.* XXXX, XXX, XXX−XXX